MODELLING OF PROPAGATING DELAMINATIONS IN TEXTILE REINFORCED DUROPLAST BEAMS BY AN ENRICHED SHELL ELEMENT FORMULATION

Jim Brouzoulis[1], Martin Fagerström[1], Johannes Främby[1], Jan Krollmann[2], and Peter Hellström[3]

[1]Department of Applied Mechanics, Division of Material and Computational Mechanics,
Chalmers University of Technology, Sweden
Email: martin.fagerstrom@chalmers.se, web page: http://www.chalmers.se

[2]Institute of Carbon Composites Dep, Technische Universität München
Boltzmannstraße 15, D-85748 Garching/München, Germany
Email: krollmann@lcc.mw.tum.de, web page: http://www.lcc.mw.tum.de/en/home/

[3]Swerea SICOMP, Material Technologies Group,
Mölndal Department, Sweden
Email: Peter.hellstrom@swerea.com, web page: http://www.swerea.se/sicomp

Keywords: Delamination, Cohesive zone, Experimental testing

ABSTRACT

Manufacturing and delamination testing, of textile reinforced Duroplast beams, have been performed to determine critical fracture energies in mode I, mode II and mixed mode loading. This includes values for growth initiation as well as propagation. For mode II and mixed mode loading, a large scatter in values were observed and no values corresponding to stable crack growth was obtained.

Furthermore, an XFEM enriched shell element, which internally can represent multiple interlaminar cracks, have been used to simulate the DCB test. In the numerical simulation, data from the experimental tests have been used as input for a bilinear cohesive zone model. The load-displacement curve from the FE analysis shows good agreement with the corresponding measured curves, although with a somewhat higher stiffness.

1 INTRODUCTION

The introduction of fiber reinforced polymers in the automotive industry is strongly dependent on accurate and efficient CAE tools to predict the correct energy absorption in car crash analyses. From experimental observations during axial crushing, cf. Grauers et al [1], it is obvious that in order to obtain good predictability in the simulations, delamination needs to be accounted for. However, due to industrial restrictions on the total simulation time of full scale crash analyses, detailed modelling of each ply as represented by separate elements through the thickness – to promote delamination modelling by cohesive interface elements – is not feasible.

In an attempt to remedy this, an enriched shell element formulation has recently been proposed with the benefit that propagating delamination cracks can be kinematically represented independently of the finite element mesh, see [2] for details. Hence, a structural model of a thin-walled laminate can thereby initially be built up by a single layer of shell elements through the thickness. During loading, the model is then enriched locally (and adaptively) in critical areas where delamination is predicted. A remaining challenge with respect to the presented enriched shell element is that the accuracy of the calculated out of plane stress components is low, hindering predictions of delamination initiation. The accuracy of the stress components is low due to a single (layered) shell element is used through the thickness to represent the laminated structure prior to delamination; therefore, we propose in this contribution to combine the enriched shell element formulation with a post-processing stress recovery of the out of plane stresses in critical areas.

To show the potential of and validate the proposed method, simulations of newly conducted delamination experiments have been conducted. For this purpose, textile reinforced duroplast beams

(matrix: Duroplast: Sika CRP 75-15, textile: Hexcel Hexforce G0926 D with fiber HTA 5131 6K) were manufactured and tested in pure mode I and II conditions (DCB and ENF) as well as under mixed mode conditions (MMB).

In this contribution, the experimental results have then been used to determine input parameters for a bilinear cohesive zone model; more precisely the critical fracture energies G_{IC}, G_{IIC} and G_C (mode mix of 0.5). In addition, the potential of using a stress recovery technique on the predictability of delamination initiation is shown together with a validation of the enriched shell element formulation by simulating a DCB test. We conclude that the proposed modeling concept is suitable for simulation of thin-walled structures undergoing substantial delaminations.

2 MANUFACTURING OF TEST SPECIMENS

To validate the developed shell element, experimental tests are necessary to derive the required fracture mechanical properties for the studied material. In the case of predicting delamination growth the interlaminar fracture energies plays a decisive role, cf. [3]. In general, the fracture energies correspond to three pure failure modes as shown in Figure 1.

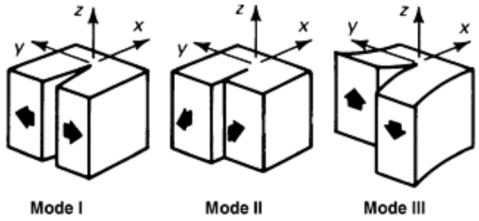

Figure 1: Modes of loading, from [4].

The experimental determination of the interlaminar fracture toughness energy G_{IC} corresponding to mode I can be realized by the double cantilever beam test (DCB). The interlaminar fracture toughness energy G_{IIC} corresponding to mode II can be determined by a test method commonly referred to as end-notch-flexure (ENF) test. Furthermore, the mixed mode bending (MMB) test represents a method that combines mode I and mode II loading, cf. [5].

2.1 Materials and processing

The manufactured test specimens are based on a polyurethane matrix system (Biresin® CRP75-15) and a woven carbon fiber reinforcement (HexForce® G0926 D 1304 TCT) with a TENAX E HTA 40 E13 fiber. The material properties for the fiber and matrix system are given in Table 1, see also [6-7].

Matrix material		Biresin® CRP75-15	HTA 40 (in fiber direction)
Young´s modulus	[MPa]	2.450	238.000
Tensile strength	[MPa]	65	3950
Elongation at break	[%]	10	1,7
Glass transition temperature	[°C]	83	-

Table 1: Material properties for the fiber and the matrix system.

All the test specimens were cut from plates consisting of a lay-up of 8 plies, 3 mm in total, with a weave orientation of 0/90°. These plates were manufactured using a vacuum assisted resin infusion process (VARI) and were infused and cured at room temperature. During the curing process, a pressure of 350 mbar was applied to obtain a fiber volume fraction of around 58%. Following this process, the plates were then tempered at 80°C for 4 hours with a heating and cooling rate of 10°C/h.

The characteristic feature of the specimen is the separation layer which serves as a predefined crack. To prevent the bonding of the layers in the notch area a stripe of Kapton® Polyimide foil with 7.5 µm thickness was placed between the middle layers of the initial plates. To simplify the removal of the PC

foil after manufacturing, the specimens was pre-treated with a release agent.

2.2 ENF Specimens

It is common practice to use the test method presented by the European Association of AeroSpace Industries (AECMA prEN 6034). In Figure 2 the used dimensions for the specimens can be seen.

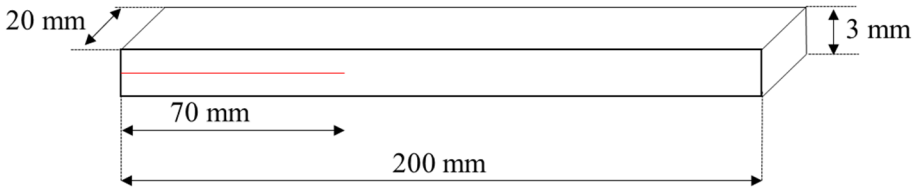

Figure 2: ENF specimen dimension with separation layer (red).

2.3 DCB & MMB Specimens

The dimensions for the DCB test specimens are specified in the standard ASTM D5528-1; however, due to a deviation (from the ASTM specification) in the way the load was introduced in the test apparatus, modifications to the test specimens were necessary, see [8], for more details.

In addition to the separation layer, grooves for the hinge caps, see Figure 3, were necessary. To realize these grooves, the fiber reinforcement of the two middle layers were reduced in length and substituted by a 1 mm polycarbonate (PC) foil, which served as a place-holder. For the MMB test the same specimens as for the DCB test were manufactured, except that the MMB specimens had an initial delamination length of 47 mm instead of 70 mm as for the DCB specimens, see ASTM D6671/D6671M-06.

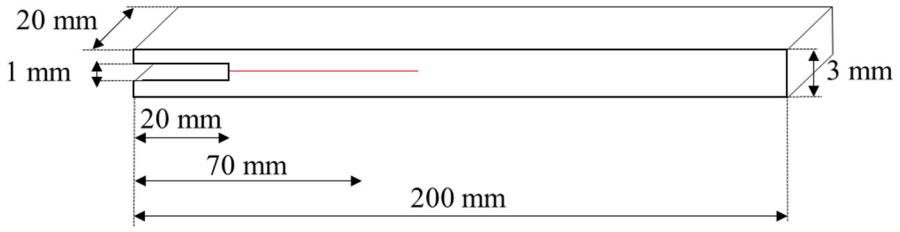

Figure 3: DCB and MMB specimen dimension with hinge cap groove and separation layer (red).

3 FRACTURE MECHANICAL TESTING

During the performed tests, the load P, displacement δ and crack tip position was recorded. An USB optical microscope was used to monitor the crack initiation and growth by tracking the crack tip. Below follows a description and results from the DCB, ENF and MMB tests.

3.1 DCB tests

Tests were performed in Mode I to determine G_{IC} according to the standard ASTM D5528-01, cf. [1]. However as was mentioned in Section 2.3, the load was introduced in a slightly different way, compared to the standard.

The specimens were loaded normal to the crack plane, at a distance c from the crack tip, and G_{IC} was then calculated using the Modified Beam Theory Method, cf. [9], according to

$$G_I = \frac{3P\delta 1000}{2b\left(a+|\Delta_{\mathrm{MBT}}|\right)} \quad [\mathrm{J/m^2}] \tag{1}$$

where P is the load, δ is the relative displacement of the load introduction points in the two cantilevers, b is the specimen width, a is the delamination length, and a correction term Δ_{MBT} This correction term is calculated for each specimen by plotting the cube root of the compliance for each crack length, and creating a linear least square root regression. The distance from the y-axis to where the regression line crosses the x-axis is equal to Δ_{MBT}.

The critical values for initiation and propagation could be determined in different ways. Two values for initiation were considered:

- The point where the deflection curve becomes nonlinear, *NL*.
- The point where the crack is visually observed to start growing, *VIS*. This is obtained by reviewing the recording from the USB microscope.

Results for initiation values, using the two methods, are presented in Table 1 for tests DCB2-6. It is observed that the *VIS* method, generally, gives lower initiation values than the *NL* method.

Specimen	NL $[\mathrm{J/m^2}]$	VIS $[\mathrm{J/m^2}]$	Δ_{MBT} [mm]
DCB 2	363	317	10.5
DCB 3	288	322	5.2
DCB 4	432	344	3.1
DCB 5	403	330	9.6
DCB 6	441	342	1.6
Average	385	331	

Table 1: Initiation values of G_{IC}

The observed abrupt decreases in load for the load-deflection curves is typical for fabrics. During propagation, a stage of somewhat stable crack growth was achieved, see Figure 4a, and the corresponding value for the fracture energy was estimated to approximately 1300 J/m^2.

As can be seen from Figure 4b, there are several abrupt decreases in the load which could possibly be explained by the fact that there are resin rich pockets, at different locations in the crack plane, giving a locally higher fracture toughness resulting in an alternation between stable and unstable crack growth.

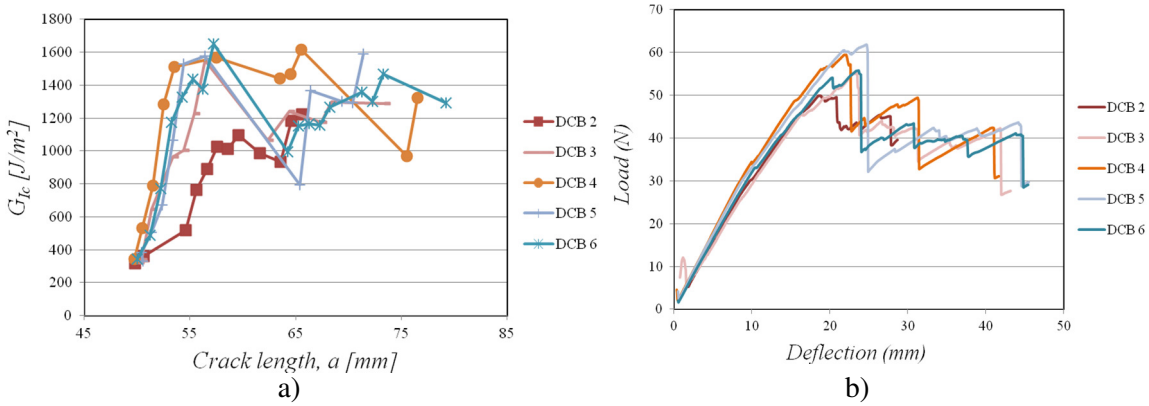

a) b)

Figure 4: a) Critical energy release G_{IC} as a function of crack length and b) load-deflection curves.

32 ENF tests

As was mentioned in Section 2.2, the ENF tests were performed according to AECMA prEN 6034. The initial crack tip is located at a distance c=35 mm from the support and the critical fracture energy for mode II crack initiation, G_{IIC}, was calculated according to

$$G_{IIC} = \frac{9Pa^2d\,1000}{2w\left(\frac{1}{4}L^3 + 3a^3\right)} \quad \left[\mathrm{J/m^2}\right] \tag{2}$$

where P is the load, a is the crack length, d the crosshead displacement, w the width of the specimen and L=100 mm is the beam span.

Specimen	G_{IIC}, VIS [J/m ^{2}]
EW1	517
EW3	737
EW4	641
EW5	623
EW6	575
Average	618

Table 2: Initiation values for G_{IIC}.

For all specimens, a steady increase in G_{IIC} was observed during propagation and, therefore, no value corresponding to stable crack growth could be obtained. It is believed that this is related to the wavy shape of the crack surfaces causing them to come into contact. The registered load-deflection curves, for all specimens, are presented in Figure 5b.

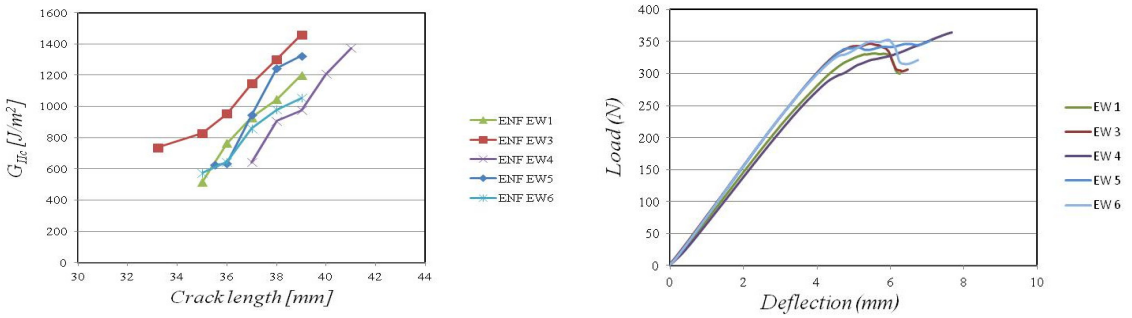

a) b)

Figure 5: a) Critical energy release G_{IIC} as a function of crack length and b) load-deflection curves.

2.3 MMB tests

The Mixed Mode Bending (MMB) tests were performed with a mode mix of 0.5, according to the ASTM D6671 standard. The span between the lower supports was 100 mm and the distance from the upper loading roller to the load introduction point was 44 mm. The test samples had an initial crack length of 30 mm. The corresponding value for the energy release G was calculated according to

$$G = G_{\mathrm{I}} + G_{\mathrm{II}} \tag{3}$$

with

$$G_I = \frac{12\left[P(3c - L) + P_g\left(3c_g - L\right)\right]^2}{16b^2h^3L^2E_{1f}}\left(a + \chi h\right)^2 \tag{4}$$

$$G_{\mathrm{II}} = \frac{9\left[P(c + L) + P_{g\left(c_g + L\right)}\right]^2}{16b^2h^3L^2E_{1f}}\left(a + 0.42\chi h\right)^2 \tag{4}$$

Where P is the load from the load cell, c is the lever arm distance set to 44 mm for these tests, L=100 mm is the free span length, P_g is the force applied by the lever arm due to its weight and c_g is the distance between the upper roller and the center of gravity of the lever arm, a is the crack length, h is the half-thickness of the specimen, b is the width. Furthermore, χ is a crack length correction parameter and is defined as

$$\chi = \sqrt{\frac{E_{11}}{11G_{13}}\left\{3-2\left(\frac{\Gamma}{1+\Gamma}\right)^2\right\}} \tag{5}$$

where

$$\Gamma = 1.18\frac{\sqrt{E_{11}E_{22}}}{G_{13}} \tag{6}$$

Here, E_{11} and E_{22} are the longitudinal and transverse modulus of elasticity respectively, and G_{13} is the out of plane shear modulus. The parameter E_{1f}, in Eq. (3)-(4), is the bending modulus of the specimen and is calculated as

$$E_{1f} = \frac{8(a_0+\chi h)^3(3c-L)^2 + \left[6(a_0+0.42\chi h)^3 + 4L^3\right](c+L)^2}{16L^2bh\left(\frac{1}{m}-C_{sys}\right)} \tag{7}$$

where m is the slope of the load displacement curve of the initial linear part of each test and C_{sys} is the compliance of the test setup.

Values for both crack initiation as well as during propagation were obtained from the MMB tests; however, no value corresponding to stable propagation was obtained. Similarly to the DCB tests, the two methods NL and VIS as described in Section 2.1 were used to determine values for initial crack growth. In Table 3 the determined values for G, for the different tests, are listed. Is should be observed that the values obtained using the VIS is generally lower than NL, as also observed for the DCB tests.

Specimen	VIS $[J/m^2]$	NL $[J/m^2]$
MMB1	364	630
MMB2	327	982
MMB3	699	592
MMB4	504	428
MMB5	447	594
MMB6	464	467
Average	468	615

Table 3: MMB initiation values.

In Figure 6a, the energy release rate G is plotted versus crack length and as can be seen from the figure, no clear stable propagation value could be obtained. Although, the two tests MMB3 and MMB4 indicate that 1700-1800 [J/m^2] could be a potential value for stable crack propagation. The load-deflection curves for the tests are shown in Figure 6b, where it should be noted that the increase in maximum loads observed for specimens MMB1 and MMB3 were due to contact between the upper and lower parts of the MMB rig.

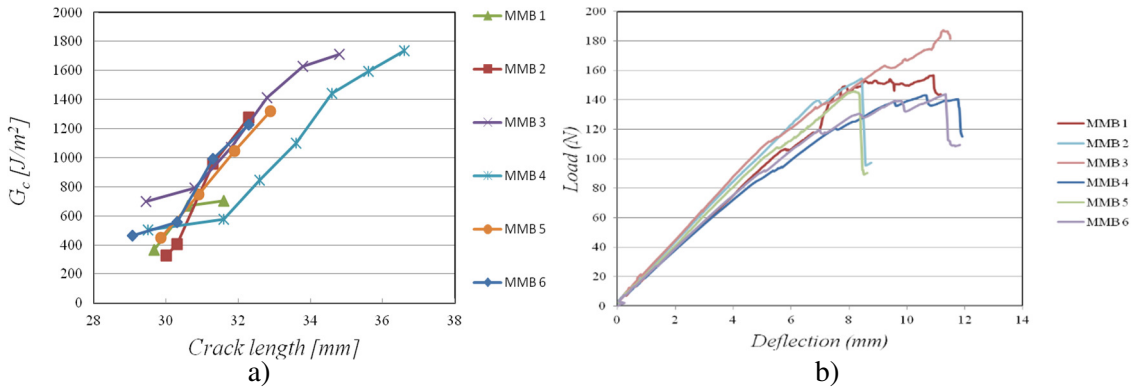

Figure 6: a) Critical energy release G_C as a function of crack length and b) load-deflection curves.

2.4 Summary of results from testing

All the determined critical fracture energies, associated with crack growth initiation and based on the VIS method, are collected in Figure 7. From the figure, the increased scatter in data for the ENF and the MMB test are clear. This scatter is attributed to the waviness of the crack surface.

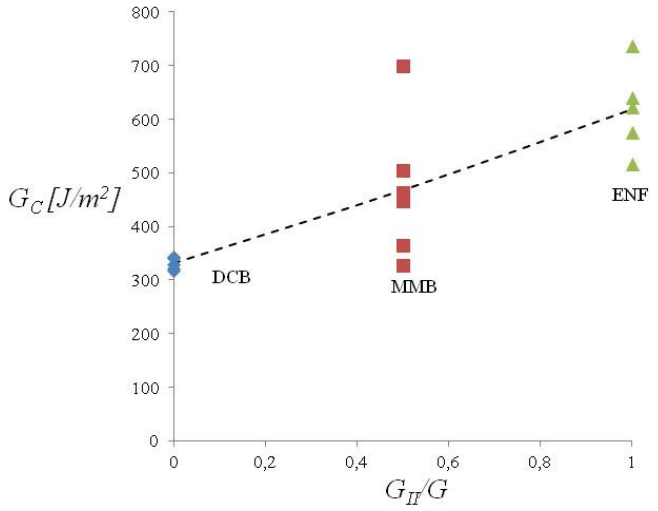

Figure 7: Collection of data showing the critical energies G_C determined from all the tests using VIS as a function of mode mix. The dashed line indicates mean values for initiation.

3 FINITE ELEMENT MODELING OF DELAMINATION TESTS

3.1 Enriched shell element

To effectively model propagation of delaminations in laminated composites, a shell element was recently developed in [2]. This element is enriched, using the eXtended Finite Element Method (XFEM), in such a manner that interlaminar cracks can med represented within the element which removes the need to model several elements on top of each other, so-called “stacking”.

In the element formulation the displacement field is approximated as a continuous (c) part and a sum of discontinuous (d) parts to represent N number of interlaminar cracks as

$$\mathbf{u} = \mathbf{u}^{\mathrm{c}} + \sum_{i=1}^{\mathrm{N}} \mathbf{u}_i^{\mathrm{d}} \tag{8}$$

Between each crack interface a cohesive zone (CZ) is introduced, to model the progressive damage evolution. In this work, a bilinear model is adopted where the critical energies in mode I and II, G_{IC} and G_{IIC} are input. In addition, the corresponding strength values are needed; however, these have not been determined from the testing and must, therefore, be assumed.

3.2 Stress recovery

To accurately predict the initiation of interlaminar cracks require the interlaminar stress state to be known; however, since shell elements are used the accuracy of these specific stress components are generally poor. To obtain a higher accuracy of these stresses, for only a small increase in computational cost, a (post-processing) stress recovery method is utilized.

To recover the interlaminar stresses, such as out-of-plane shear and normal stresses, the equations of equilibrium can be integrated in the thickness direction which leads to

$$\begin{cases} \tau_{xz} = -\int_{-\frac{h}{2}}^{z} \left(\sigma_{xx,x} + \tau_{xy,x}\right) \mathrm{d}z \\ \tau_{yz} = -\int_{-\frac{h}{2}}^{z} \left(\sigma_{yy,y} + \tau_{xy,y}\right) \mathrm{d}z \end{cases} \tag{9}$$

Then in a second step, based on the recovered shear stresses above the out-of-plane normal stress can be recovered in a similar manner as

$$\sigma_{zz} = -\int_{\frac{h}{2}}^{z} \left(\tau_{xz,x} + \tau_{yz,y}\right) \mathrm{d}z \tag{10}$$

To evaluate the integrals, the stress gradients above need to be determined. One natural choice, and also adopted in this work, is to project the stresses to the nodes and then use the shape functions of the element to evaluate the gradients.

In Figure 8, an example of the current stress recovery method is illustrated for a laminate beam. There, the transverse shear and normal stresses are shown for the shell element solution together with the recovered stresses and a reference solution (based on 3D modeling). It is concluded that the accuracy is very much improved.

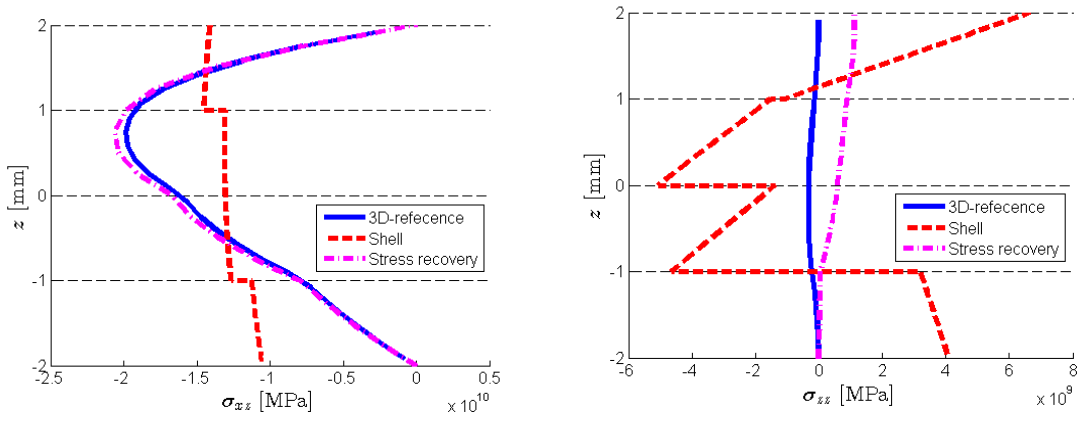

a) b)

Figure 8: Comparison of transversal stresses in an asymmetric 4-ply beam. a) shows transverse shear stress and b) shows transverse normal stress.

3.4 Validation of FE modeling by simulation of DCB testing

Here, we utilize the adopted shell element to simulate progressive delamination in a DCB test with the aim to validate the element. Since the crack path is known (for this example), there is no need for the proposed stress recovery method and it will, therefore, be omitted.

For the cohesive zone model, the fracture energy in mode I is set to G_{IC} = 1300 J/m^2 (according to Section 3.1) and the strength of the zone in the normal direction is estimated as σ_{fn} = 60 MPa from [10].

In Figure 9, the simulated load-displacement curve (FEM) is shown for together with the measured DCB curves. As can be seen from the figure, relatively good agreement is observed between simulation and experiment, although with a somewhat stiffer response for the FE simulation. It should also be noted that the waviness of the fracture surface is not considered; something that potentially can be modeled using friction in the cohesive zone.

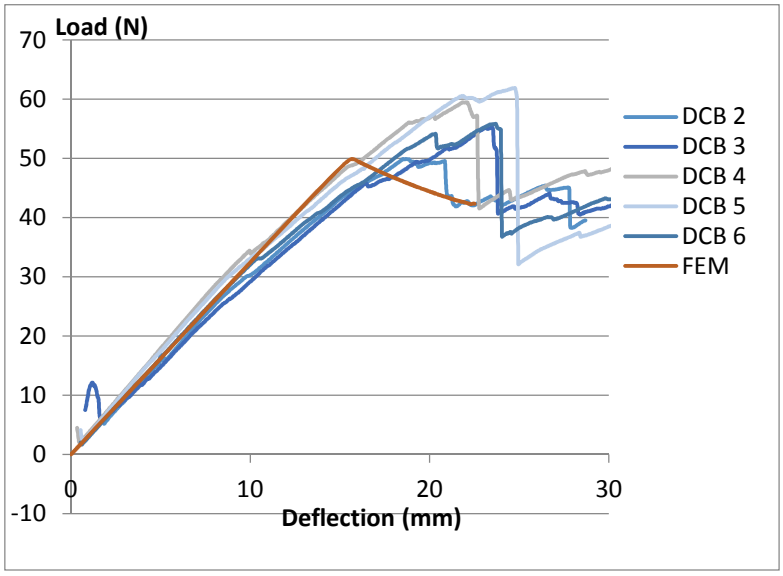

Figure 9: Load-displacement curves from measured DCB tests together with an FE simulated curve.

4 CONCLUSIONS

This paper presents manufacturing, testing and FE simulation of textile reinforced Duroplast beams (matrix: Duroplast: Sika CRP 75-15, textile: Hexcel Hexforce G0926 D with fiber HTA 5131 6K). The aim of the testing was to determine critical fracture energies corresponding to initiation and progressive delamination. Therefore, the test specimens were tested in mode I (DCB), mode II (ENF) and mixed mode (MMB).

Regarding fracture energy for initiation, values showing small scatter was obtained for the DCB tests whereas there was much larger scatter for the ENF and MMB tests. Since the specimens were manufactured from a fabric the resulting fracture surfaces were/are wavy, which for tests that include a mode II component implies contact between the crack surfaces. Consequently, this is considered to be the reason for the increased scatter.

From the FE modeling of the DCB testing, it was seen that good agreement between simulated and measured load- deflection curves were obtained. This validates the proposed shell element for this mode of loading.

ACKNOWLEDGEMENTS

The research leading to these results receives funding from the European Communities Seventh Framework Programme (FP7/2007-2013), under grant agreements no. 314182 (the MATISSE project) and no. 314567 (the ENLIGHT project). This publication solely reflects the authors' views. The European Community is not liable for any use that may be made of the information contained herein.

REFERENCES

[1] L. Grauers, R. Olsson, R. Gutkin, Energy absorption and damage mechanisms in progressive crushing of corrugated NCF laminates: Fractographic analysis, Composite Structures; 110:110-117, (2014).

[2] J. Brouzoulis, M. Fagerström An enriched shell element formulation for efficient modeling of multiple delamination propagation in laminates. *Composite Structures*; 126:196-206, (2015).

[3] ASM Handbook Committee, *ASM HandBook,* Mechanical Testing and Evaluation, Vol. 8, ASM International, 2000.

[4] P. P. Camanho, C. G. Davila, S. T. Pinho, J. J. C. Remmers, *Mechanical Response of Composites*, Vol. 10 Springer, 2008.

[5] J. Reeder, J. R. Jr Crews, Mixed-Mode Bending Method for Delamination Testing, *AIAA Journal, Volume 28, Number 7, July 1990, pp. 1270—1276.*

[6] Toho Tenax Co., Ltd., Delivery and characteristics for Tenax® HTA filament yarn, http://www.tohotenax-eu.com/fileadmin/tohotenax/downloads/Produkte/Technische%20Datenblaetter/HTA40%20%26%20HTS40%20dt.pdf (24.03.2015).

[7] Sika AG, PUR-Composite-System CRP-75-15 Material Data Sheet (available upon request)

[8] Brandt F. (1998). New load introduction concept for improved and simplified delamination beam testing. *J Experimental Techniques*; 22(1):17-20.

[9] Juntti M., Asp L.E., Olsson R., Assessment of evaluating Methods for the Mixed-Mode Bending Test, J. of Composites Technology and Research, JCTRER, Vol. 21, No. 1, 1999, pp. 37-48.

[10] Ganter Otto GmbH & Co KG, Material characteristics of Duroplast and Technopolymer, http://www.ganter-griff.com/uploads/tx_rldownloadlist/characteristics_of_duroplast_-_technopolymer.pdf (28.04.2015).